Physical Properties and Sensing Properties of Iron (II) Ion-Doped Zinc Sulfide Nanostructured Thin Films Deposited via Chemical Spray Pyrolysis

Zainab Al-Ramadhan[1], Raghad Hamdan Mohsin[2], Abeer Ghalib Hadi[2], Shaymaa A. Hussein[3], Sami Salman Chiad[1], Nadir Fadhil Habubi[1,4,5] and Yassin Hasan Kadhim[6]

[1] *Department of Physics, College of Education, Mustansiriyah University, 10052 Baghdad, Iraq*
[2]*General Directorate of Education in Baghdad Governorate, Rusafa Second, Ministry of Education, 10021 Baghdad, Iraq*
[3]*Department of Medical Laboratory Techniques, Al-Manara College for Medical Science, 62001 Al-Amarah, Iraq*
[4]*Department of Radiation and Sonar Technologies, Alnukhba University College, 10013 Baghdad, Iraq*
[5]*Department of Radiology Techniques, Al-Qalam University College, 36001 Kirkuk, Iraq*
[6]*Department of Optics Techniques, College of Health and Medical Techniques, AL-Mustaqbal University, 51001 Hillah, Babylon, Iraq*
dr.sami@uomustansiriyah.edu.iq, dr.zainabphysics@uomustansiriyah.edu.iq, beerghalibhadia@gmail.com

Keywords: ZnS, Fe, Thin Films, XRD, AFM, Optical Properties, Bandgap.

Abstract: Nanostructured thin films of Iron (Fe)-doped Zinc Sulfide (ZnS) were deposited via the Chemical Spray Pyrolysis (CSP) technique, with varying concentrations of Iron incorporated into the ZnS matrix. XRD analysis confirmed that all films preserved a zinc blende cubic structure, while the calculated average crystallite size increased from 13.25 nm for pure ZnS to 14.8 nm for Fe-doped samples. The structural investigation further demonstrated that Iron incorporation influenced lattice parameters, microstrain, and dislocation density, thereby reflecting measurable changes in overall crystal quality. Atomic Force Microscopy (AFM) revealed a relatively smooth and uniform surface topography, supporting the good quality of the prepared thin films. Optical properties were systematically examined using UV-Visible spectroscopy, which showed a clear dependence of band gap energies on Fe concentration, indicating that Fe ions effectively substituted Zn sites. Gas sensing measurements toward NO_2 at 125°C highlighted that Fe doping generally reduced sensitivity; however, thinner films exhibited enhanced responsiveness due to their larger surface-to-volume ratio and the presence of more active interaction sites. These results suggest potential for tailoring ZnS-based materials in optoelectronic and sensing applications.

1 INTRODUCTION

ZnS is the quintessential II-VI semiconductor, showcasing two primary crystalline structures. Zinc (Zn) and sulfur (S) in each variation maintain a tetrahedral coordination geometry. The more prevalent cubic variant, often called zinc blende or sphalerite, epitomizes stability [1]-[2]. Conversely, the hexagonal manifestation is recognized as wurtzite. At 300 Kelvin, zinc blende boasts a bandgap of approximately 3.54 eV, while wurtzite exhibits a slightly wider bandgap of about 3.91 eV. ZnS, being intrinsic, can be doped to function as either n-type or p-type semiconductors [3]-[4]. The II-VI semiconductor group, to which ZnS belongs, presents intriguing optical properties that are size-tunable [3], [5]-[7]. Doped nanomaterials garner significant attention due to their broad applicability across various devices, including solar cells, sensors, optical communication systems, (LEDs), and infrared detectors, among others [8]-[9] ZnS has been doped with Cr, Fe, and Ni, [10]. Notably, the ionic radius of Fe^{2+} (0.77 Å) closely resembles that of Zn^{2+} (0.74 Å), recommending that Fe^{2+} can readily integrate into the ZnS lattice or substitute Zn^{2+} [11]. Doping ZnS can significantly alter its properties, particularly in the case of transition metal co-activated ZnS nanostructures, which represent a novel class of luminescent materials. Various techniques for thin film deposition are commonly employed, including CVD) [12], (CBD) [13], [14], PVD) [15], electrodeposition [16], sol-gel [17], spin coating [18], and CSP [19]. CSP stands out for its simplicity, cost-

effectiveness, and scalability to large-area processing, offering low fabrication costs.

2 EXPERIMENTAL

Thin films of ZnS and Fe-doped ZnS were grown onto preheated glass substrates using the CSP technique. A matrix solution for the ZnS thin films was prepared by dissolving 0.1M $ZnCl_2$ (sourced from Merck Chemicals) in deionized water. To introduce Fe doping, aqueous solutions containing 0.1M $FeCl_3$ (obtained from Merck Chemicals) in deionized water were prepared to achieve volumetric percentages of 2% and 4% Fe doping. These solutions were then added to the matrix to obtain the desired 2% and 4% Fe-doped samples. The preparation conditions were optimized: For the duration of the deposition procedure, the base temperature remained at 450°C. The carrier gas was N2, with a deposit rate of 4 mL/min. To prevent rapid cooling, the spraying was conducted at a rate of 10 seconds, followed by a 1-minute interval. The discharge was maintained at a distance of 30 cm from the substrate. The weighing method was employed for estimating the film thickness, which was found to be 320 ± 20 nm. XRD was employed to obtain structural parameters via a Shimadzu XRD-6000 instrument,. The surface topography was investigated using AFM. Transmittance was measured using a double-beam spectrophotometer. The percentage variation in resistance within a cylindrical chamber (radius: 8.5 cm, height: 18 cm) was used to evaluate gas sensitivity.

2 RESULTS AND DISCUSSIONS

Figure 1 displays the XRD patterns. Peaks are observed at 28.42°, 33.07°, 47.62°, and 59.23°, respectively, which match with ICDD card No (5-0566), confirming a cubic zinc blend structure for ZnS. The corresponding reflecting planes are identified as (111), (200), (220), and (222), respectively. Additionally, the broadening of the XRD pattern provide an indication for creation of nanostructured thin films. The (200) peak exhibits maximum intensity at 33.07° in the event that 4% Fe films, a slight increase in peak intensity is observed at 28.42°, 33.07°, 47.62°, and 59.23°, respectively. This could be attributed to the substitution of smaller Zn^{2+} ions (0.74 Å) with larger Fe^{2+} ions (0.77 Å) [20], [21]. Besides the characteristic peaks of ZnS, no additional peaks related to Fe or its complex oxides were detected. The (200) plane typically exhibits maximum intensity in the hexagonal wurtzite structure, In other words, the ratio of ZnS to Fe increases with higher tin incorporation, suggesting a more ordered structure. This enhanced structural ordering may also increase film growth rates, further enhanced by Fe doping [22], [23].The crystallite sizes (D) of all compositions of ZnS: Fe nanostructure films were calculated via (1) [24].

$$D = \frac{K\lambda}{\beta cos\theta}. \quad (1)$$

where k = 0.89, λ =1.54 Å, β denotes FWHM for prominent (200) peak, and θ represents Bragg's angle of diffraction. The alteration in FWHM is directly correlated with the crystallite size and various other structural factors, which have been computed and summarized in Table 1. Based on the XRD analysis, it is evident that the determined crystallite size, FWHM, defect concentrations indicated by microstrain, and dislocation density all increase with higher iron content [25], [26]. This indicates that the incorporation of Iron disrupts the lattice of the host ZnS, causing the crystallite size to rise as a result of the substitutes of smaller Zn^{2+} ions with larger Fe^{2+} ions. The highest crystallinity was achieved with the largest grain size of 14.8 nm. The agglomeration of Fe clusters that do not replace the Zn^{2+} ions [27]-[30] could be the cause of the increase in *D* for doping values of 2% and 4%.The microstrain (ε) in the film is determined by (2) [31]:

$$\varepsilon = \frac{\beta cos\theta}{4}. \quad (2)$$

The dislocation density (δ) was obtained via (3) [32]:

$$\delta = \frac{1}{D^2}. \quad (3)$$

The decline in ε and δ with rising doping content up to 4 at% suggests an improvement in the structural stability of the films. At the minimum values of ε and δ, carriers encountered less resistance within the lattice, facilitating their unrestricted movement [33], [34]. This phenomenon indicates improved conductivity and mobility of charge carriers within the material. It's widely acknowledged that ε and δ tend to decrease as *D* increases (see Table 1). This trend reflects a more ordered and defect-free lattice structure associated with larger crystallite sizes, reducing ε and δ [35], [36].

Table 1: Structural parameters of pure ZnS and doping with Fe films.

Specimen	2 θ	hkl	FWHM (°)	E_g eV	*D* nm	$\delta \times 10^{14}$	ε 10^{-4}
Undoped ZnS	33.07	200	0.63	3.46	13.1	57.6	26.3
ZnS: 2% Fe	33.05	200	0.60	3.40	13.8	52.3	25.0
ZnS: 4% Fe	33.00	200	0.56	3.34	14.80	45.6	23.4

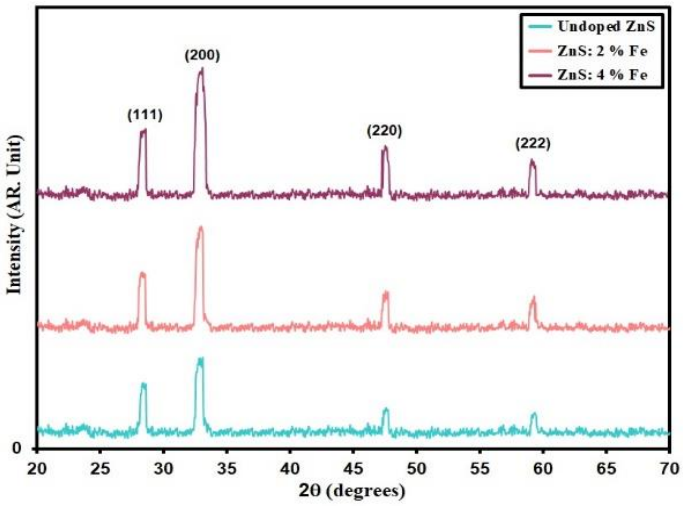

Figure 1: XRD styles of grown films.

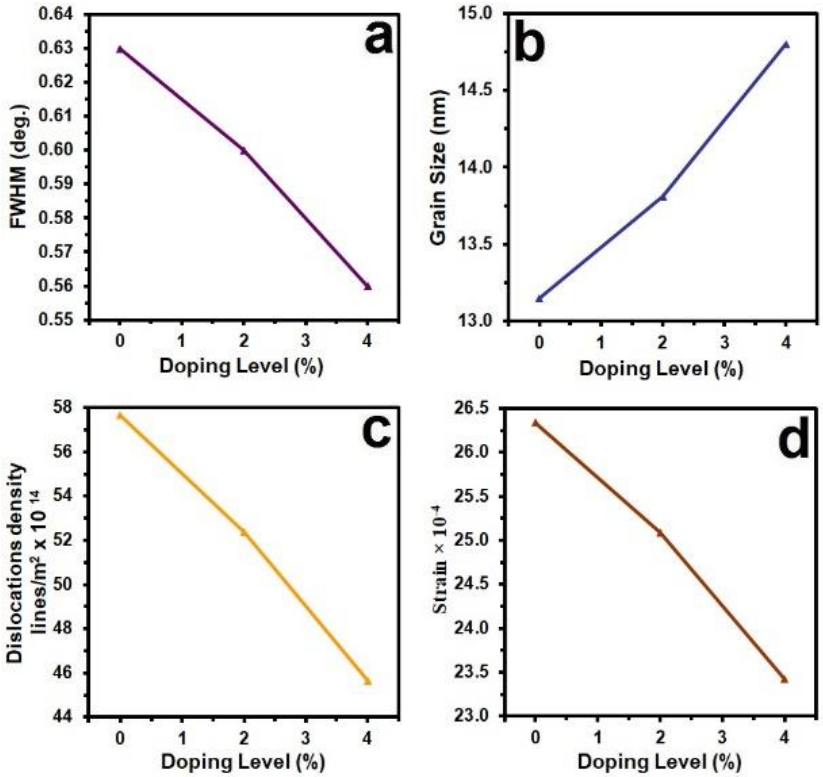

Figure 2: Structural parameters of the enteded films.

Atomic Force Microscopy (AFM) provides a powerful tool for obtaining microscopic insights into surface structures and generating topographic maps representing surface morphology. This method provides digital pictures that make it easier to assess surface properties quantitatively., such as root mean square roughness (rms) or average roughness (R_a). It allows for analyzing images from various perspectives, including two-dimensional simulation. Figure 2 depicts a 1µm×1µm AFM micrograph of Fe-doped ZnS thin films fabricated via the CSP process. The two-dimensional AFM images illustrate that the surfaces of all thin films, whether ZnS or ZnS:Fe, are composed of densely packed, with no voids, pinholes, or cracks detected. The average particle size is measured at 88.9 nm, decreasing to 44.1 nm with 4% Fe doping [37], [38]. The average grain size in diameter for ZnS:Fe (0%, 2%, and 4%) is listed in Table 2. From Figure 3, Ra and rms values of (10.14, 8.95, and 4.12) nm and (9.81, 5.39, and 4.26) nm were determined for surface roughness with molarity [39, 40]. It is observed from Table 2 that the average particle size, Ra, and rms values decrease with increasing doping concentration for all samples.

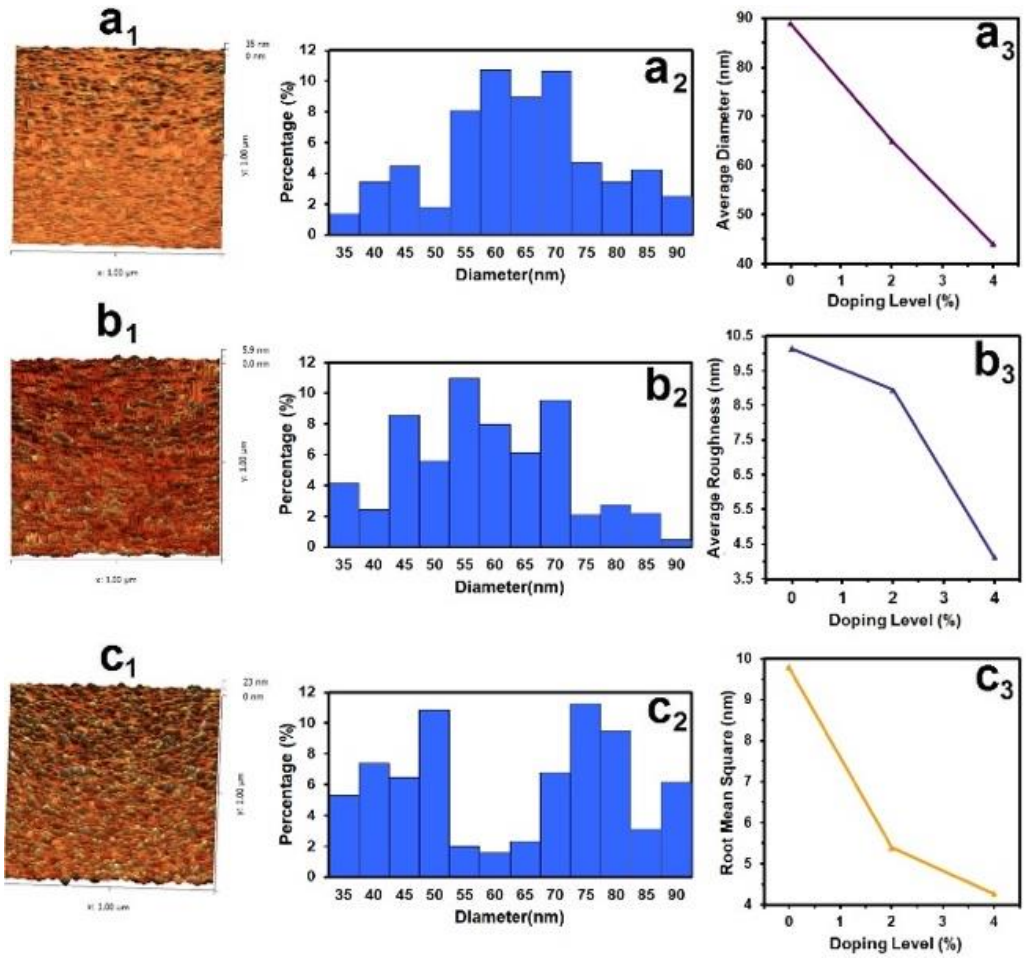

Figure 3: AFM information.

Table 2: AFM parameters of the intended films.

Samples	Average Particle size nm	R_a (nm)	rms (nm)
Undoped ZnS	88.9	10.14	9.81
ZnS: 2% Fe	65.0	8.95	5.39
ZnS: 4% Fe	44.1	4.12	4.26

UV-Vis spectroscopy is a straightforward and valuable method for characterizing thin films.

Figure 4 and Figure 5 depict the transmittance (T) and absorbance (A) spectra of the deposit films. The thin films exhibit reduced transparency beyond wavelengths of 350 nm. Moreover, the pronounced rise in T spectra between 320 nm and 350 nm indicates the crystal structure is uniform and compact [41], [42]. Figure 5 demonstrates that the absorption threshold is detected at 240 nm for ZnS. However, doped ZnS thin films exhibit a notable shift in the UV-visible spectra, with absorption peaks shifting to higher wavelengths at 300 nm (2% doping) and 400 nm (4% doping). The maximum and minimum absorption edge are attributed to variations in the size of the nanostructured films [43], [44].

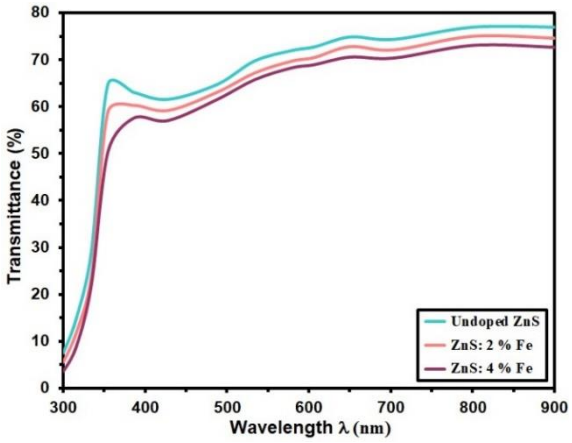

Figure 4: Transmittance (T) of the entended films.

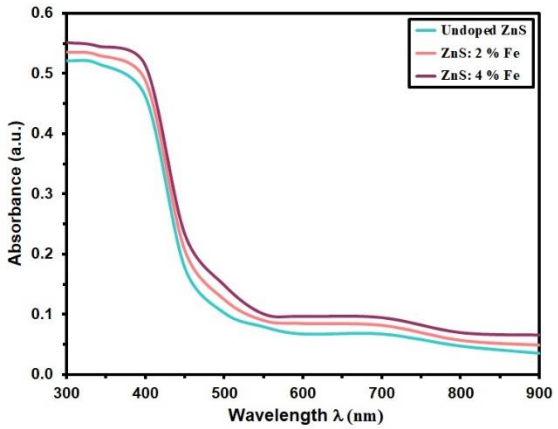

Figure 5: Absorbance (A) of the entended films.

Figure 6 shows that the absorption coefficient (α) was > 10^4 cm^{-1}. The absorption edge shifted towards the photon energy (hν) region with an increase in Fe content up to 2%. The presence of unsaturated bonds in the layers may contribute to the formation of defects [45], [46].

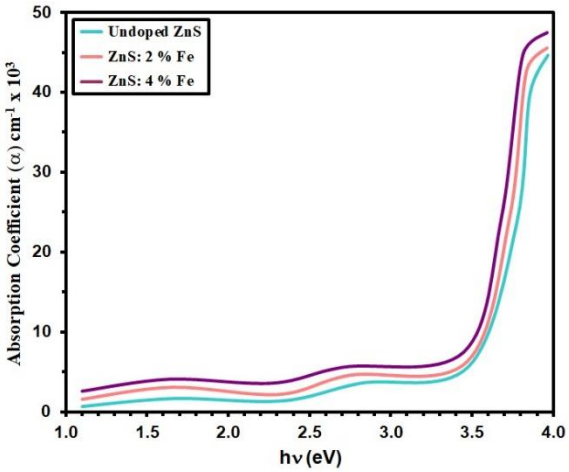

Figure 6: Absorption coefficient (α) of the deposit films.

The relationship between α and hν can be expressed as [47]:

$$\alpha h\nu = B(h\nu - E_g)^r. \quad (4)$$

Here, E_g represents the band gap, B is constant, and the exponent (r) = ½ corresponding to The direct band gap Figure 7 illustrates E_g values for ZnS and doped ZnS.

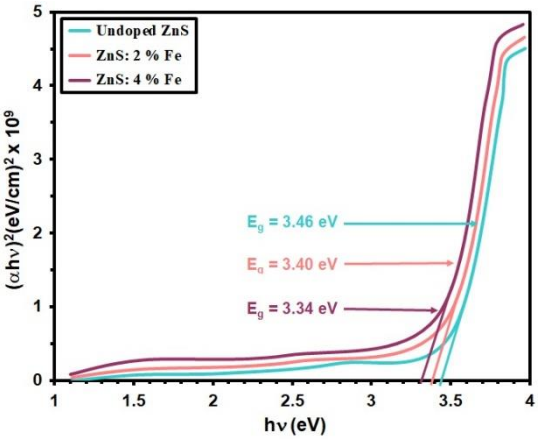

Figure 7: The gap energy (E_g) of the deposit films.

It is apparent that E_g for ZnS:Fe thin films decreases from 3.84 to 3.64 eV with an increase in ZnS:Fe molar doping from 2% to 4%, respectively.[48], [49] The trend that has been noticed can be ascribed to the enlargement of nanocrystal size, as evidenced by XRD analysis. The increase in nanocrystal size leads to a decline in E_g, which is in line with the size dependency observed in

semiconductor materials [50].The refractive index (n) was determined via (5) [51]:

$$n = \frac{1+R^{\frac{1}{2}}}{1-R^{\frac{1}{2}}}. \quad (5)$$

The extinction coefficient was evaluated via (6) [52]:

$$k = \frac{\alpha\lambda}{4\pi}. \quad (6)$$

where R is reflectance. Figure 8 shows that n decreases slightly with variations in doping concentration, ranging from 2.80 to 2.62 at a wavelength of 336 nm. The films' n and kvalues decrease with rising wavelength. n decreases as the wavelength increases, stabilizing at higher wavelengths, and indicating normal dispersion behavior [53], [54]. Upon observing Figures 8 and 9, it's apparent that n values remain constant at 550 nm and at longer wavelengths. N affects the optical path of light and influences the amount of light reflected from a surface. The extinction coefficients of the films reach minimum values in the wavelength range of 600-900 nm.

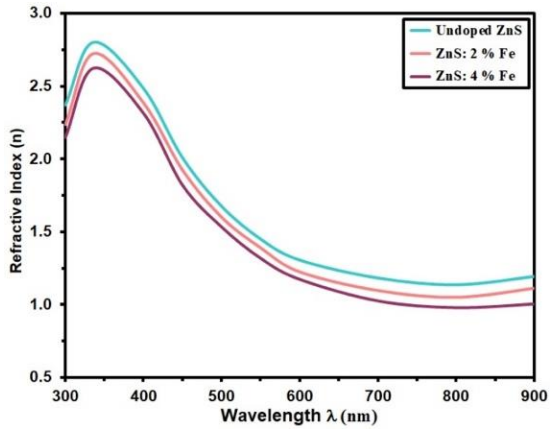

Figure 8: Refractive index (n) of te deposit films.

The ZnS film's capability to detect NO_2 gas is illustrated by the increase in resistance it experiences when exposed to the gas at a temperature of 125°C [55], [56]. This increase in resistance is due to the interaction between NO_2 molecules and the ZnS film, which alters the film's electrical conductivity. Typically, NO_2 molecules capture free charge carriers from the film, reducing their concentration and causing an increase in resistance. Additionally, Fe dopant in ZnS film could further influence its gas-sensing properties, potentially enhancing or reducing sensitivity. Figure 10 likely presents the gas response curves for ZnS and ZnS: Fe films, which provide visual data on their gas-sensing behavior [57], [58].

The sensor's response (s) can be quantified using the (7) [59]:

$$\text{Sensitivity} = \frac{\Delta R}{R_g} = \left|\frac{R_g - R_a}{R_g}\right| \times 100\ \%. \quad (7)$$

Figure 11 shows s of ZnS and ZnS films doped with 2% and 4% Fe to various NO_2 gas concentrations (50, 100, and 150 ppm). As doping concentration increases, sensitivity decreases, likely due to hindered gas diffusion caused by the doping elements [60]. The ZnS: 4% Fe films display the lowest sensitivity, possibly because the Fe ions obstruct gas diffusion, reducing the sensor's efficiency. The observed decline in sensitivity across different NO_2 concentrations further suggests that thinner ZnS films exhibit better responsiveness to NO_2 gas, likely due to a higher surface area and improved gas interaction [61].

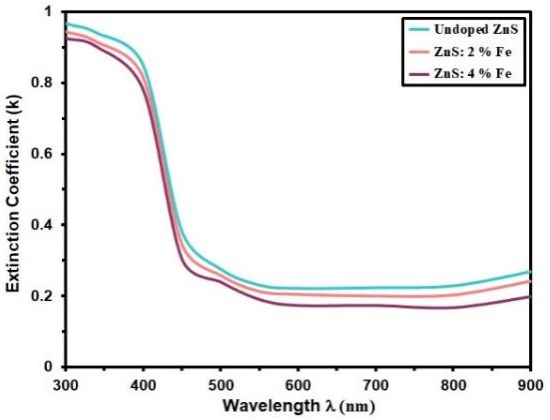

Figure 9: Extinction coefficient (k) of the deposit films.

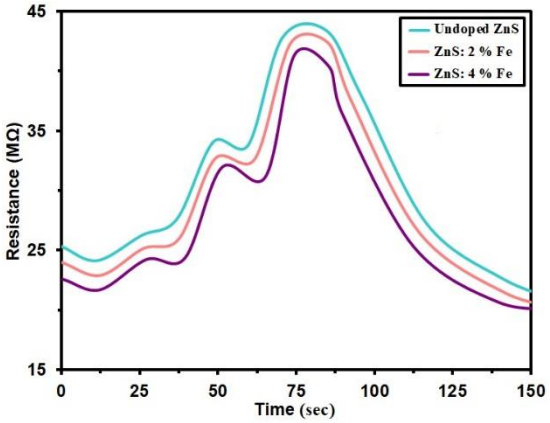

Figure 10: Illustrates resistance over time for undoped ZnS and ZnS: Fe films with various dopant concentrations.

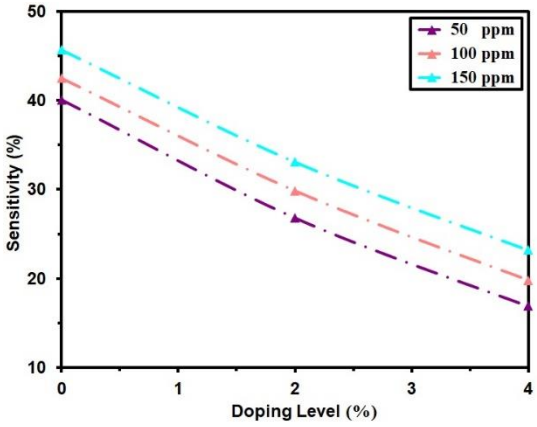

Figure 11: Displays the sensitivity of undoped ZnS and ZnS: Fe films with varying dopant concentrations.

4. CONCLUSIONS

The study successfully demonstrates the impact of Fe doping on the structural, morphological, optical, and gas sensing properties of ZnS nanostructured thin films synthesized via chemical spray pyrolysis. XRD analysis confirmed a zinc blende cubic phase for all films, with a slight increase in crystallite size and improved crystallinity upon doping. The incorporation of Fe ions led to a decrease in microstrain and dislocation density, indicating enhanced structural quality. AFM analysis showed that surface roughness and particle size decreased with increasing Fe content, with the 4% Fe-doped sample exhibiting the smoothest surface morphology. Optical studies revealed high transmittance in the visible range, with a noticeable redshift in the absorption edge and a reduction in bandgap energy from 3.84 eV to 3.64 eV due to the enlargement of nanocrystal size. The refractive index and extinction coefficient varied with wavelength and doping concentration, confirming direct bandgap behavior and normal dispersion characteristics. In terms of gas sensing, the films exhibited increased resistance upon NO_2 exposure, confirming their sensitivity. However, higher Fe doping led to reduced sensitivity, likely due to obstructed gas diffusion. Despite this, thinner Fe-doped films showed enhanced responsiveness due to their larger surface area and increased active sites.

ACKNOWLEDGMENTS

This effort was supported by Mustansiriyah University.

REFERENCES

[1] I. Yu, T. Isobe, and M. Senna, Optical properties and characteristics of ZnS nano-particles with homogeneous Mn distribution. Journal of Physics and Chemistry of Solids, vol. 57, no. 4, p. 373, 1996.

[2] V. L. Colvin, M. C. Schlamp, and A. P. Alivisatos, "Light-emitting diodes made from cadmium selenide nanocrystals and a semiconducting polymer," Nature, vol. 370, pp. 354–357, 1994.

[3] A. P. Alivisatos, "Semiconductor clusters, nanocrystals and quantum dots," Science, vol. 271, no. 5251, pp. 933–937, 1996.

[4] W. G. Becker and A. J. Band, "Photoluminescence and photoinduced oxygen adsorption of colloidal zinc sulphide dispersions," J. Phys. Chem., vol. 87, pp. 4888-4893, 1983.

[5] A. A. Green and M. C. Hersam, "Colored semitransparent conductive coatings consisting of monodisperse metallic single-walled carbon nanotubes," Nano Lett., vol. 8, pp. 1417-1422, 2008.

[6] S. Kar and S. Biswas, "White light emission from surface oxidized manganese-doped ZnS nanorods," J. Phys. Chem. C, vol. 112, pp. 11144-11149, 2008.

[7] H. C. Ong and R. P. H. Chang, "Optical constants of wurtzite ZnS thin films determined by spectroscopic ellipsometry," Appl. Phys. Lett., vol. 79, pp. 3612-3614, 2011.

[8] G. Nabiyouni, R. Sahraei, M. Toghiany, M. H. Majles Ara, and K. Hedayati, "Preparation and Characterization of Nano-Structured ZnS Thin Films Grown on Glass and N-Type Si Substrates Using a New Chemical Bath Deposition Technique," Rev. Adv. Mater. Sci., vol. 27, pp. 52-57, 2011.

[9] R. John and S. Sasiflrence, "Optical, Structural and Morphological Studies of Bean-Like ZnS Nanostructures," Chalcogenide Lett., vol. 7, pp. 269-273, 2010.

[10] R. D. McNorton, T. A. Schuler, J. M. MacLaren, and R. A. Stern, "Systematic trends of first-principles electronic structure computations of Zn(1-x)A(x)B diluted magnetic semiconductors," Phys. Rev. B, vol. 78, no. 7, 2008.

[11] M. S. Akhtar, S. Riaz, S. S. Hussain, and S. Naseem, "Magnetic properties of un-doped and Fe-doped ZnS thin films," Advances in Civil, Environmental and Materials Research, Busan, Korea, pp. 24-28, 2014.

[12] V. G. Bessergeneva, E. N. Ivanovaa, Y. A. Kovalevskayaa, S. A. Gromilova, V. N. Kirichenkoa, S. M. Zemskovaa, I. G. Vasilievaa, B. M. Ayupova, and N. L. Shwarz, "Optical and structural properties of ZnS and ZnS:Mn films prepared by CVD method," Materials Research Bulletin, vol. 30, no. 11, pp. 1393-1400, 1995.

[13] M. H. Suhail, "Structural and optical properties of ZnS, PbS, Zn1-xPbxS, ZnxPb1-xS and PbZnxS1-x thin films," Indian J. Pure Appl. Phys., vol. 50, pp. 380-386, 2012.

[14] P. A. Luque, M. A. Quevedo-Lopez, and A. Olivas, "Influence of deposition time on ZnS thin film growth over SiO2 and glass substrates," Mater. Lett., vol. 106, pp. 49-51, 2013.

[15] P. Kumar, A. Kumar, P. N. Dixit, and T. P. Sharma, "Optical, structural and electrical properties of zinc sulphide vacuum evaporated thin film," Indian J. Pure Appl. Phys., vol. 44, no. 9, pp. 690-693, 2006.

[16] A. S. Baranski, M. S. Bennet, and W. R. Fawcett, "The physical properties of ZnS thin films electrodeposited from aqueous diethylene glycol solutions," J. Appl. Phys., vol. 54, no. 11, pp. 6390-6394, 1983.

[17] W. Daranfed, M. S. Aida, A. Hafdallah, and H. Lekiket, "Substrate temperature influence on ZnS thin films prepared by ultrasonic spray," Thin Solid Films, vol. 518, no. 4, pp. 1082-1084, 2009.

[18] T. M. Thi, N. T. Hien, D. X. Thu, and V. Q. Trung, "Thin films containing Mn-doped ZnS nanocrystals synthesized by chemical method and study of some of their optical properties," J. Exp. Nanoscience, vol. 8, no. 5, pp. 694-702, 2012.

[19] E. Turan, M. Zor, A. S. Aybek, and M. Kul, "Electrical properties of ZnO/Au/ZnS/Au films deposited by ultrasonic spray pyrolysis," Thin Solid Films, vol. 515, no. 24, pp. 8752-8755, 2007.

[20] M. S. Akhtar, M. A. Malik, Y. G. Alghamdi, K. S. Ahmad, S. R. Riaz, and S. Naseem, "Chemical bath deposition of Fe-doped ZnS thin films: Investigations of their ferromagnetic and half-metallic properties," Mater. Sci. Semicond. Process., vol. 39, pp. 283-291, 2015.

[21] S. Vijayalakshmi, S. Venkataraj, and R. Jayavel, "Facile fabrication of CuO nanoparticles via spray pyrolysis," J. Phys. D: Appl. Phys., vol. 41, p. 245403, 2008.

[22] A. Nakrela, N. Benramdane, A. Bouzidi, Z. Kebbab, M. Medles, and C. Mathieu, "Site location of Al-dopant in ZnO lattice by exploiting the structural and optical characterisation of ZnO:Al thin films," Results Phys., vol. 6, p. 133, 2016.

[23] H. T. Salloom, E. H. Hadi, N. F. Habubi, S. S. Chiad, M. Jadan, and J. S. Addasi, "Characterization of silver content upon properties of nanostructured nickel oxide thin films," Digest Journal of Nanomaterials and Biostructures, vol. 15, no. 4, pp. 1189-1195, 2020.

[24] S. B. Majumder, M. Jain, and R. S. Katiyar, "Investigations on the optical properties of sol–gel derived thin films," Thin Solid Films, vol. 402, pp. 90-98, 2002.

[25] A. S. Edelestein and R. C. Camarata, Nanomaterials Synthesis Properties and Application, Institute of Physics Publishing, London, U.K., 1998.

[26] A. Martynes, C. Guillen, and J. Herrero, "Structural and optical properties studies of ZnS thin films," Applied Surface Science, vol. 140, p. 182, 1999.

[27] K. Santhosh Kumar, C. Manoharan, S. Dhanapandian, and A. Gowri Manohari, "Effect of Sb dopant on the structural, optical and electrical properties of SnS thin films by spray pyrolysis technique," Spectrochim. Acta A: Mol. Biomol. Spectrosc., vol. 115, pp. 840-844, 2013.

[28] R. Sahraei and S. Darafarin, "An investigation on optical characteristics of nanocrystalline ZnS:Ni thin films prepared by chemical deposition method," Spectrochim. Acta A: Mol. Biomol. Spectrosc., vol. 149, pp. 941-948, 2015.

[29] R. Mohd Ibrahim, M. Markom, and K. F. Abd Razak, "Optical properties of Fe2+ ion doped ZnS nanoparticles synthesized using co-precipitation method," Jurnal Kejuruteraan, vol. 27, pp. 87-94, 2015.

[30] R. S. Ali, N. A. H. Al Aaraji, E. H. Hadi, K. H. Abass, N. F. Habubi, and S. S. Chiad, "Effect of lithium on structural and optical properties of nanostructured CuS thin films," Journal of Nanostructures, vol. 10, no. 4, pp. 810-816, 2020.

[31] M. Devika, N. K. Reddy, K. Ramesh, K. R. Gunasekhar, E. S. R. Gopal, and K. T. R. Reddy, J. Electrochem. Soc., vol. 153, pp. G727-G733, 2006.

[32] T. S. Moss, Optical Properties of Solids, Butterworths, London, 1961.

[33] F. Aghaei, R. Sahraei, E. Soheyli, and A. Daneshfar, "Dopant-concentration dependent optical and structural properties of Cu-doped ZnS thin films," J. Nanostruct., vol. 12, no. 2, pp. 330-342, 2022.

[34] M. D. Giello, M. Miccocci, R. Rella, P. Siciano, and A. Tepore, Thin Solid Films, vol. 148, pp. 273-278, 1987.

[35] B. Subramanian, C. Sanjeeviraja, and M. Jayachandran, Mater. Chem. Phys., vol. 71, pp. 40-46, 2001.

[36] A. Jrad, T. Ben Nasr, and N. Turki-Kamoun, "Study of structural, optical and photoluminescence properties of indium-doped zinc sulfide thin films for optoelectronic applications," Opt. Mater., vol. 50, p. 128, 2015.

[37] K. Wright, G. W. Watson, S. C. Parker, and D. J. Vaughan, "Simulation of the structure and stability of sphalerite (ZnS) surfaces," Am. Mineral., vol. 83, pp. 141-146, 1998.

[38] B. D. Cullity, Answers to Problems: Elements of X-ray Diffraction, Addison-Wesley, Boston, MA, USA, 1978.

[39] G. Jauncey, "The scattering of x-rays and Bragg's law," Proc. Natl. Acad. Sci. USA, vol. 10, pp. 57-60, 1924.

[40] B. Elidrissi, M. Addou, M. Regragui, A. Bougrine, A. Kachouane, and J. Bernède, "Structure, composition and optical properties of ZnS thin films prepared by spray pyrolysis," Mater. Chem. Phys., vol. 68, pp. 175-179, 2001.

[41] A. K. Kole and P. Kumbhakar, "Cubic-to-hexagonal phase transition and optical properties of chemically synthesized ZnS nanocrystals," Results Phys., vol. 2, pp. 150-155, 2012.

[42] M. Ashrat, M. Mehmood, and A. Qayyum, "Influence of source-to-substrate distance on the properties of ZnS films grown by close-space sublimation," Semiconductors, vol. 46, pp. 1326-1330, 2012.

[43] K. Benyahia, A. Benhaya, and M. S. Aida, "ZnS thin films deposition by thermal evaporation for photovoltaic applications," J. Semicond., vol. 36, p. 103001, 2015.

[44] F. Özütok, K. Ertürk, and V. Bilgin, "Growth, electrical, and optical study of ZnS:Mn thin films," Acta Phys. Pol. A, vol. 121, pp. 1-3, 2012.

[45] A. Derbali, A. Attaf, H. Saidi, M. Aida, H. Benamra, R. Attaf, N. Attaf, and H. Ezzaouia, "Br doping effect on structural, optical and electrical properties of ZnS thin films deposited by ultrasonic spray," Mater. Sci. Eng. B, vol. 268, p. 115135, 2021.

[46] Z. Zhang, D. Shen, J. Zhang, C. Shan, Y. Lu, Y. Liu, B. Li, D. Zhao, B. Yao, and X. Fan, "The growth of single cubic phase ZnS thin films on silica glass by plasma-assisted metalorganic chemical vapor deposition," Thin Solid Films, vol. 513, pp. 114-117, 2006.

[47] R. S. Ali, M. K. Mohammed, A. A. Khadayeir, Z. M. Abood, N. F. Habubi, and S. S. Chiad, "Structural and optical characterization of sprayed nanostructured indium doped Fe2O3 thin films," J. Phys.: Conf. Ser., vol. 1664, no. 1, 012016, 2020.

[48] A. El Hichou, M. Addou, J. L. Bubendorff, J. Ebothé, B. El Idrissi, and M. Troyon, "Microstructure and cathodoluminescence study of sprayed Al and Sn doped ZnS thin films," Semicond. Sci. Technol., vol. 19, p. 230, 2003.

[49] G. Gordillo and E. Romero, "Structural characterization of thin films based on II–VI ternary compounds deposited by evaporation," Thin Solid Films, vol. 484, pp. 352-357, 2005.

[50] M. Ashraf, S. M. J. Akhtar, M. Mehmood, and A. Qayyum, "Optical and structural properties of ZnSxSe1−x thin films deposited by thermal evaporation," Eur. Phys. J. Appl. Phys., vol. 48, p. 4, 2009.

[51] A. A. Khadayeir, R. I. Jasim, S. H. Jumaah, N. F. Habubi, and S. S. Chiad, "Influence of substrate temperature on physical properties of nanostructured ZnS thin films," J. Phys.: Conf. Ser., vol. 1664, no. 1, 2020.

[52] S. S. Chiad, A. S. Alkelaby, and K. S. Sharba, "Optical conduct of nanostructure Co3O4 rich highly doping Co3O4:Zn alloys," Journal of Global Pharma Technology, vol. 11, no. 7, pp. 662-665, 2020.

[53] C. Jin, H. Kim, K. Baek, and C. Lee, "Effects of coating and thermal annealing on the photoluminescence properties of ZnS/ZnO one-dimensional radial heterostructures," Mater. Sci. Eng. B, vol. 170, pp. 143-148, 2010.

[54] M. Caglar, Y. Caglar, and S. Ilican, "Investigation of the effect of Mg doping for improvements of optical and electrical properties," Physica B, vol. 485, p. 6, 2016.

[55] P. Bhuvaneswari and M. Velusamy, "Effect of fluorine doping on the structural, optical and electrical properties of spray deposited cadmium stannate thin films," Mater. Sci. Semicond. Process., vol. 16, pp. 1964-1970, 2013.

[56] T. Mahalingam, V. Dhanasekaran, G. Ravi, S. Lee, J. P. Chu, and H. J. Lim, "Effect of deposition potential on the physical properties of electrodeposited CuO thin films," J. Optoelectron. Adv. Mater., vol. 12, no. 6, pp. 1327-1332, 2010.

[57] S. S. Chiad, H. A. Noor, O. M. Abdulmunem, and N. F. Habubi, "Optical and structural properties of Ni-doped Co3O4 nanostructure thin films via CSPM," J. Phys.: Conf. Ser., vol. 1362, no. 1, 2019.

[58] M. Motallebi Aghgonbad and H. Sedghi, "Influence of annealing temperature on optical properties of zinc oxide thin films analyzed by spectroscopic ellipsometry method," Chin. J. Phys., vol. 56, pp. 2129-2138, 2018.

[59] K. Haleh and M. M. A., "Deposition-rate dependence of optical properties of titanium nanolayers," J. Phys. Opt., vol. 13, pp. 4-11, 2012.

[60] J. Yuvaloshin, S. Ra, and G. Ravi, "Effect of annealing on optical and structural properties of ZnS/MnS and MnS/ZnS superlattices thin films for solar energy application," J. Opt., vol. 125, pp. 1775-1779, 2014.

[61] M. Motallebi Aghgonbad and H. Sedghi, "Spectroscopic-ellipsometry measurement of the optical properties of zinc oxide thin films prepared by sol–gel method: coating speed effect," Micro & Nano Lett., vol. 13, pp. 959-964, 2018.